Available online at www.sciencedirect.com
ScienceDirect
Journal of Molecular Graphics and Modelling 26 (2007) 558–570
Journal of Molecular Graphics and Modelling
www.elsevier.com/locate/JMGM

Structural analysis of lead fullerene-based inhibitor bound to human immunodeficiency virus type 1 protease in solution from molecular dynamics simulations

Vannajan S. Lee [a,*], Piyarat Nimmanpipug [a], Ornjira Aruksakunwong [b], Siriporn Promsri [c], Pornthep Sompornpisut [c], Supot Hannongbua [c,**]

[a] Department of Chemistry, Faculty of Science, Chiang Mai University, Chiang Mai 50200, Thailand
[b] Department of Chemistry, Faculty of Science, Rangsit University, Pathumtani 12000, Thailand
[c] Department of Chemistry, Faculty of Science, Chulalongkorn University, Bangkok 10330, Thailand

Received 15 December 2006; received in revised form 16 March 2007; accepted 30 March 2007
Available online 4 April 2007

Abstract

Molecular dynamics (MD) simulations of the HIV-1 protease (HIVP) complexed with lead fullerene-based inhibitor (diphenyl C_{60} alcohol) in the three protonated states, unprotonated (Un-), monoprotonated (Mono-), and diprotonated (Di-) states at Asp25 and Asp25′ were performed. As the X-ray structure of the investigated complex is not available, it was built up starting with the X-ray crystallographic structure of the HIVP complexed with non-peptide inhibitor (PDB code: 1AID) and that of the diphenyl C_{60} alcohol optimized using the integrated ONIOM molecular orbital calculations. The inhibitor was, then, introduced into the enzyme pocket using a molecular docking method. Change of the HIVP binding cavity for all three states were evaluated in terms of distance between the two catalytic residues, Asp25 and Asp25′ as well as those between the catalytic residues and the flap regions. The torsional angles formed by the O–C–C–O of the two carboxyl groups of the catalytic dyad show the non-planar configuration with the most frequency at about −45° for the Un-, 35° and −95° for the Mono- and 60° for the Di-systems. At equilibrium, different orientations of the fullerene-based inhibitor in the three protonation states were observed. For the Di-state, the OH group of the inhibitor stably forms hydrogen bonds with the two aspartic residues. It turns to the flap region to form hydrogen bonding to the backbone N of Ile50′ for the Un-state. In contrast, the OH group turns to locate between the catalytic and the flap region for the Mono-states. Beside the molecular orientation, the rotation of the OH group of the inhibitor in the Un-state was also detected. In terms of solvation, the carboxylate oxygens of the aspartic residues in the Un- and Mono-states were solvated by one to three water molecules while the OH group in these two states was coordinated by one water molecule. This is in contrast to the Di-state in which no water molecule is available in the radius of 5–6 Å around the oxygen atoms of the carboxylate groups of enzyme and of the OH group of the inhibitor. The simulated results lead to the conclusion that the active site of the HIVP complexed with the diphenyl C_{60} alcohol is the diprotonation states on Asp25 and Asp25′.

Keywords: MD simulations; Fullerene-based inhibitors; HIV-1 protease; Molecular docking

1. Introduction

A number of potent and selective HIVP inhibitors have been developed and approved as drugs for the treatment of HIV infection. Most of these are peptidic such as saquinavir, ritonavir, etc. Efforts have been made in several laboratories to develop non-peptide-based HIVP inhibitors. One of these, which was a novel water-soluble fullerene derivative was proposed on the basis of modeling and then synthesized by Wudl, Friedman and coworkers in 1993 [1,2]. Although, the size of C_{60} fullerene looks very large for a drug, it is only one nanometer in diameter, roughly the size of many small pharmaceutical molecules. The ability of C_{60} fullerene derivatives to interact with the active site of HIV-1 protease has been examined through simple physical chemical analysis. Kinetic analysis of HIVP in the presence of various water-soluble C_{60} derivatives suggests a competitive

* Corresponding author. Tel.: +66 53 943341x117; fax: +66 53 892277.
** Corresponding author. Tel.: +66 22 187602; fax: +66 22 187603.
E-mail addresses: vannajan@chiangmai.ac.th, vannajan@gmail.com (V.S. Lee), supot.h@chula.ac.th (S. Hannongbua).

1093-3263/$ – see front matter © 2007 Elsevier Inc. All rights reserved.
doi:10.1016/j.jmgm.2007.03.013

mode of inhibition because of the ability to form bonds with the catalytic aspartic acids in addition to van der Waals contacts with the non-polar HIVP surface, thereby improving the binding.

Various functionalizations have been utilized both to increase the hydrophilicity (e.g. –OH, –COOH, $–NH_2$) and to prepare new compounds presenting biological and pharmacological activity. The inhibition values were promising with K_i in the range between 103 nM and 5.5 μM [3] and EC_{50} from 0.21 to 2.60 μM [4] in comparison with K_i of indinavir (0.14 nM), nelfinavir (0.28 nM), ritonavir (0.17 nM) and saquinavir (0.15 nM) [5]. The high level of solubility in water (34 mg/ml at pH 7.4) has been obtained by Hirsch and coworkers [6], who synthesized a dendrimeric fullerene derivative bearing 18 carboxylic groups ($EC_{50} = 0.22$ μM). Note that the solubility of amprenavir in water is 0.04 mg/ml. *In vitro* studies of a water-soluble fullerene derivative (diphenethylamino-succinate methano-C_{60}) with a peripheral blood mononuclear cell (PBMC) confirmed its inhibition ability with an EC_{50} of 7 μM. Such a compound has reached the same level of potency of the peptidomimetic inhibitors.

Diphenyl C_{60} alcohol, the best potency of C_{60} derivative, in current form is probably too non-polar to be a drug. However, due to a large portion of the molecule that could be modified, it offers the opportunity to synthesize new derivatives to enhance its binding affinity, solubility, toxicity, and bioavailability. Indeed, many antiviral fullerene drugs show good in vitro antiviral activity and lack of toxicity at concentrations up to approximately 100 μM [7–9] in comparison with the commercially available drugs such as amprenavir, indinavir, ritonavir, atazanavir, saquinavir, nelfinavir and lopinavir ($CC_{50} \approx 4.49$–4.95 μM) [10]. The total surface area of diphenyl C_{60} alcohol of 485 $Å^2$ is directly comparable to that of typical clinically used HIVP inhibitors, e.g., indinavir, 544 $Å^2$ as reported by Friedman et al. [3]. Although it has a relatively high molecular weight and density of packing of the atoms in the fullerene core determines its interactions with solvent and protein. This is comparable to clinically relevant compounds.

X-ray studies of structures of HIVP complexed with peptide or peptide analog inhibitors indicate substantial conformational changes of an enzyme upon binding, i.e., a very large movement of the flaps upon the size of the inhibitor bound at the active site, is often reported from both theoretical and experimental studies [11–17]. These significant changes indicate a role of structural dynamics in inhibitor-enzyme binding. Ma et al. and Carlson and McCammon and references therein [18,19] reviewed the recent methods, which incorporate protein flexibility to understand the complex nature of ligand–receptor binding.

A number of potent fullerene-based inhibitors were studied and patented [4,20–25]. However, an X-ray crystal structure of HIVP complexed with fullerene derivatives is not yet available. The first microscopic level prediction of the tight closing of the flexible flaps, when a novel C_{60}-based inhibitor is docked into the Un-, Mono-, and Di-protonated states of the active site of HIVP, was investigated by Zhu et al. [26] using molecular dynamics simulations. The simulations addressed the exclusion of water density near the flap regions, around the active-site region and in the cavity as well as the changes in the shape of the cavity in order to accommodate the inhibitor. This reduction of water leads to an enhancement of the hydrophobic interaction between the C_{60} moiety and the interior of the cavity, including the flaps. This finding is consistent with that of Friedman et al. [3], that the activity of an inhibitor compound can be improved by maximizing the amount of hydrophobic surface area. The simulations indicated, also, that the most effective binding of fullerene-based inhibitors to the active site takes place when the Asp dyad is diprotonated. The suggestion agreed well with the ^{13}C NMR experiment of the pepstatin A/HIVP complex reported by Smith et al. [27] and the *ab initio* molecular dynamics calculations by Piana et al. [28].

Besides, the issue of the connection between flap motion, specifically flap-closing and favorable inhibition of the HIVP was also addressed by Simmerling and coworkers [29–31] using molecular dynamics simulations. In this study, cyclic urea inhibitor was embedded into the open state of free protease. It was found that the HIVP flaps were changed spontaneously to the closed conformation.

To investigated in more detail, we studied the binding of HIVP and the best potency of C_{60} derivative, diphenyl C_{60} alcohol, with $K_i = 103$ nM according to Friedman et al. [3]. The structure analysis parameters such as internal motion of the inhibitor's torsional angles as well as rotation of the inhibitor, itself, its location within the cavity and an analysis of the hydrogen bonding between the inhibitor and the active-site Asp residues were reported from our simulations. We performed 1200 ps molecular dynamics simulations of the complexes for the three protonated states, unprotonated (Un-), monoprotonated at Ash25 (Mono-) and diprotonated at both Ash25 and Ash25′ (Di-). The results revealed an insight into the structural origins of binding strength, binding orientation, the flap motion, the possible relationship between binding and catalytic efficiency, and the numbers as well as orientation of water molecules in the HIVP cavity site.

2. Computational methods

2.1. Preparation of HIVP

Since the X-ray crystallographic structure of the HIVP complexed with the fullerene-based inhibitors has never been published, the initial HIVP structure was taken from the HIVP complexed with haloperidol derivative at 2.2 Å resolutions (1AID entry in PDB database) [32]. This structure is a class of HIVP non-peptide inhibitor complex and has a large cavity site (about 10 Å), which can accommodate the fullerene spheroid (about 7 Å). Its structure is considered to be in the ''closed'' form according to Simmerling and coworkers [29–31] where the flaps are pulled in toward the bottom of the active site. The HIVP cavity was defined as the distance from the tip of the flap (O atom of Gly48) to the catalytic oxygen (O atom of Gly27) for both two chains of the dimer. The structural water as well as the inhibitor was, then, removed. All hydrogen atoms were added into the structure. Ionization states for all other ionizable residues (except for Asp25/25′) were assigned according to the

standard pK_a values of amino acids, i.e. Glu^{-1}, Asp^{-1}, Arg^{+1}, Lys^{+1} and His^{+1}. A short minimization run was performed in order to remove any potentially bad contacts using the program package AMBER, Version 7 [33,34]. This minimization using 5000 steps for the steepest descent method and then 5000 steps for the conjugate gradient method was employed without any constraints. A dielectric constant of 1 was used. A cutoff distance at 12 Å for non-bonded interactions was applied.

2.2. Preparation of diphenyl C_{60} alcohol structure

The geometry of the diphenyl C_{60} alcohol was optimized using the multi-layered integration method, known as the ONIOM method. At a high level, the density functional theory (DFT), B3LYP/6-31G*, was applied for the atoms of the side chain (ball and stick in Fig. 1) while the PM3 calculation was used for all atoms [35].

2.3. Molecular docking of HIVP, fullerene-based inhibitor complex

The initial unprotonated structure of the HIVP–diphenyl C_{60} alcohol complex was obtained using a molecular docking method. The reliability of the docking approach was performed by docking saquinavir into the HIVP cavity. The result is comparable to that of the X-ray structure of the complex. The docking of the C_{60} buckyball with HIVP was, then, performed in order to approximate a good orientation of the inhibitor in the enzyme cavity. The unprotonated Asp25/Asp25′ were used. Gasteiger charges were employed for both inhibitor and HIVP atoms. Grid maps were calculated using the module AutoGrid in AutoDock 3.0 program [36–38] for the protease structure. The docking of C_{60} (buckyball) with HIVP was initially performed in order to get a good approximation of center of cavity in order to avoid any symmetry problems that might arise. The center of mass in the Cartesian coordinate of the lowest energy conformation of the C_{60} was, then, used as the center of grid. A number of grid points in *x*-, *y*-, and *z*-coordinate are 60, 60, 60, respectively, with the spacing of 0.375 Å. This parameter set covers the active site of the enzyme and allows the inhibitor to move and explore the enzyme active site without any constraint. The search method is the Metropolis Monte Carlo and simulated annealing algorithms. The docking structure with the best rank, the lowest interaction free energies among the highest population set, was subsequently used by substituting the fullerene with the diphenyl C_{60} alcohol. In this step, two approaches, automatic and manual dockings, were employed. In automatic docking, we followed the same procedure described above. For the latter approach, the OH group of the diphenyl C_{60} alcohol was manually put toward the carboxylate side chain of the two catalytic residues and a short minimization for fine-tuning was, then, applied. This manual docking approach relies on the fact that the hydroxyl isostere of the HIVP inhibitors essentially forms hydrogen bonds with the Asp25/Asp25′ [39–41].

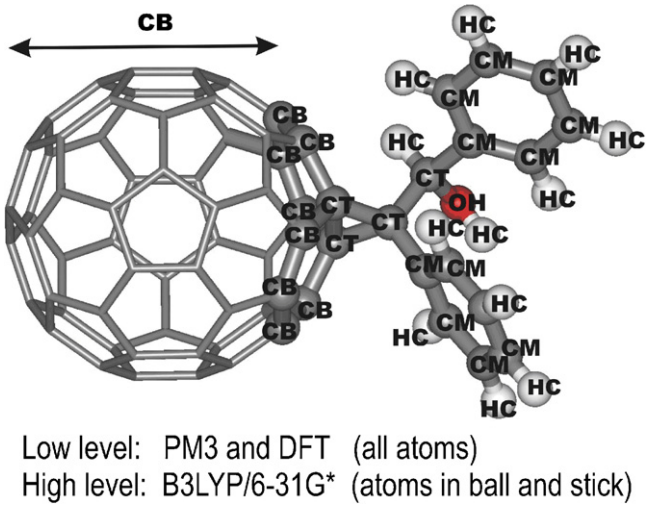

Fig. 1. Optimal geometry of the diphenyl C_{60} alcohol obtained from ONIOM calculations where their force fields were assigned by the labeled atom types (see text for more details).

2.4. Molecular dynamic simulations

The energy minimized conformation of the HIVP–diphenyl C_{60} complex of the unprotonated system (Un-), where the OH group of diphenyl C_{60} alcohol points directly to the catalytic site of the enzyme, was used as the starting structure. Then, the other two systems, mono-protonated (Mono-) at aspartic acid chain B (Ash25′) and the diprotonated (Di-) at Ash25 and Ash25′ of both chains, were generated. The molecular mechanics potential energy minimizations and MD simulations were carried out using the program package AMBER, Version 7. Calculations were performed using the parm99 force field reference for the HIVP and the diphenyl C_{60} alcohol. The atom types for the diphenyl C_{60} alcohol were assigned (Fig. 1) by mapping their chemical properties (element, hybridization, bonding schemes) to the AMBER atom type library. For the atomic net charges, the Gasteiger values were used.

Most of the rigid carbon atoms of the C_{60} spheroid were assigned as CB AMBER atom type and carbons at the triangle bridge were assigned as CT. The other atom types such as OH, CM, HC and HO for sp^3 oxygen in alcohol, sp^2 carbon, hydrogen attached to aliphatic carbon and hydrogen in alcohol were, respectively, defined and shown in Fig. 1. The enzyme–inhibitor complex was solvated, 10 Å from the molecular surface. The simulated systems were treated under periodic boundary conditions and an isobaric–isothermal ensemble (NPT) at 1 atm and constant temperature of 298 K. The volume was chosen to maintain a density of 1 g/cm^3. A cutoff distance of 12 Å was applied for non-bonded pair interaction. The Particle Mesh Ewald method was employed for correcting electrostatic interactions beyond the cutoff. The counter ions were added to neutralize the system. The potential energy minimizations were performed on the system using 5000 steps of steepest descent method with position restraint applied for the inhibitor atoms. A dielectric constant of 1 was used. For the MD simulations, the temperature of the system was gradually increased by heating from 0 to 298 K for the first 60 ps and kept constant according to the Berendsen algorithm [42] at 298 K

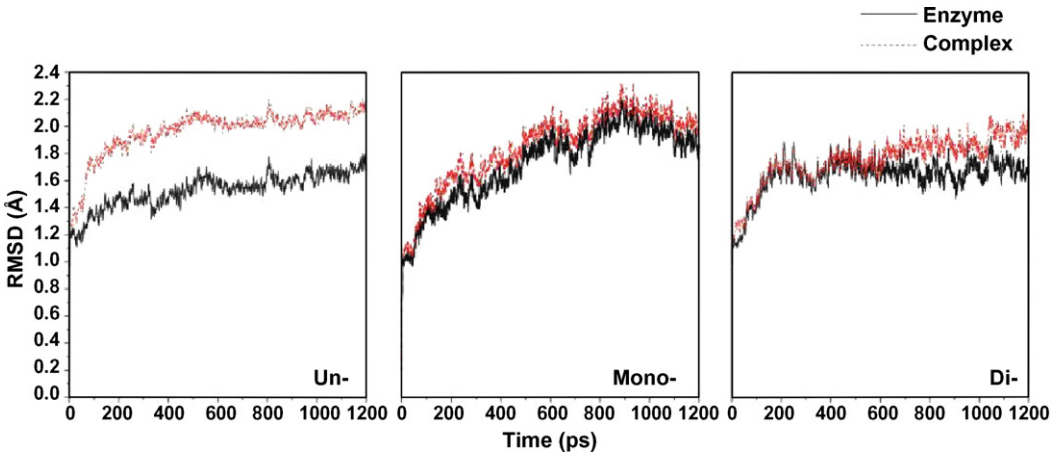

Fig. 2. Root mean square displacement (RMSD) of the HIVP enzyme and its complex with the diphenyl C_{60} alcohol relative to the initial minimized structure of the unprotonated (Un-), monoprotonated (Mono-) and diprotonated (Di-) systems.

from 61 to 1200 ps. The simulation time step of 2 fs was used. The configurations of the system were collected between 400 and 1200 ps. A snapshot of trajectory was stored every 0.1 ps for later analysis.

3. Results and discussions

3.1. Characteristic of the MD simulations

In the present study, the initial ligand/enzyme geometry for the unprotonated system was derived using the rigid molecular docking method followed by short minimization. It is known that the OH group of almost all HIVP inhibitors, if available, was observed to bind directly to the carbonyl group of the catalytic dyad, Asp25 and Asp25′ [39–41]. This is not the case for the investigated systems in which the OH group cannot move through the energy barrier due to the rigidity of the two catalytic residues in the automatic docking procedure. To examine this evidence, the OH group of the diphenyl C_{60} alcohol was manually turned to bind to the aspatic's carbonyl. The inhibitor/enzyme stabilization energies for the two initial states, the automatic docking and the manually oriented ones, were calculated, subtract the total energy of the complex by the sum of the total energy of the enzyme and the inhibitor-based on the molecular mechanics (MM) force field embedded in the AMBER program. The obtained results for the automatic and the manual structures are 6.90 and −39.3 kcal/mol, respectively. It can be seen that the latter structure MM structure is in a much lower energy state in comparison to that of the former structure.

Starting from the initial structure of the unprononated complex where the OH functional group of the diphenyl C_{60} alcohol points toward the catalytic dyad of the HIVP, one and two hydrogen atoms were added to the aspatic's carboxylate group. The energy minimized structures of these complexes yielded the stabilization energies of −59.1 and −52.9 kcal/mol for the Mono- and Di-protonated states, respectively.

The total potential energy and kinetic energy over simulation time was examined and shown that equilibrium was reached after 400 ps. This is consistent with the root mean square displacements (RMSD) of all protein atoms over the 1.2 ns trajectory calculated in comparison to the initial minimized structure of the complex (Fig. 2). The average RMSD plots for the three systems are in the range 1.40–2.20 Å. Separation between the two lines, RMSDs of the enzyme and of the complex, was found only for the unprotonated state (Fig. 2a). The RMSD for all atoms of enzyme in the Un-state is slightly lower than that of the Di- and Mono-states, respectively. This indicates less conformational change, compared to the initial structure, of the enzyme in the Un- than the other two states. Significant increase of the RMSD in the Un-state of the complex over that of the enzyme indicates flexibility of the diphenyl C_{60} alcohol due, as expected, to a loose binding between the inhibitor in the unprotonated enzyme. This can be the reason for the separation between the enzyme's and the complex's RMSDs, which takes place only for the Un- state. Superimposition of the final MD structures of the three systems using C_α backbone of enzyme (Fig. 3)

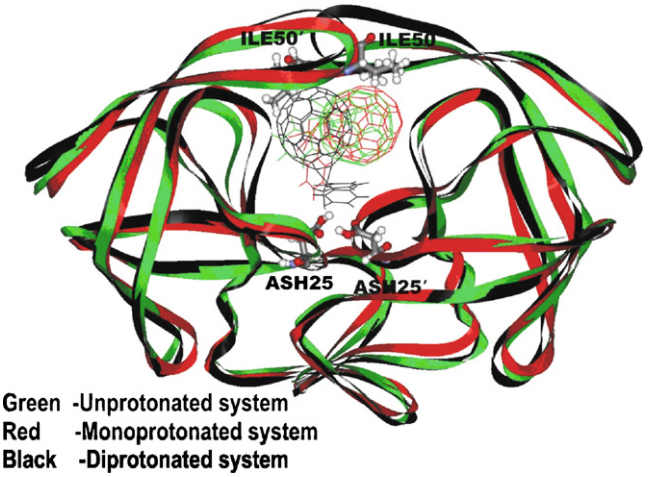

Fig. 3. Superimposition of Cα enzyme backbone of the final MD structures for the unprotonated (green), monoprotonated (red) and diprotonated (black) systems where the Asp25 and Asp25′ residues at the catalytic site and the Ile50 and Ile50′ at the flap region were labeled as ball and stick.

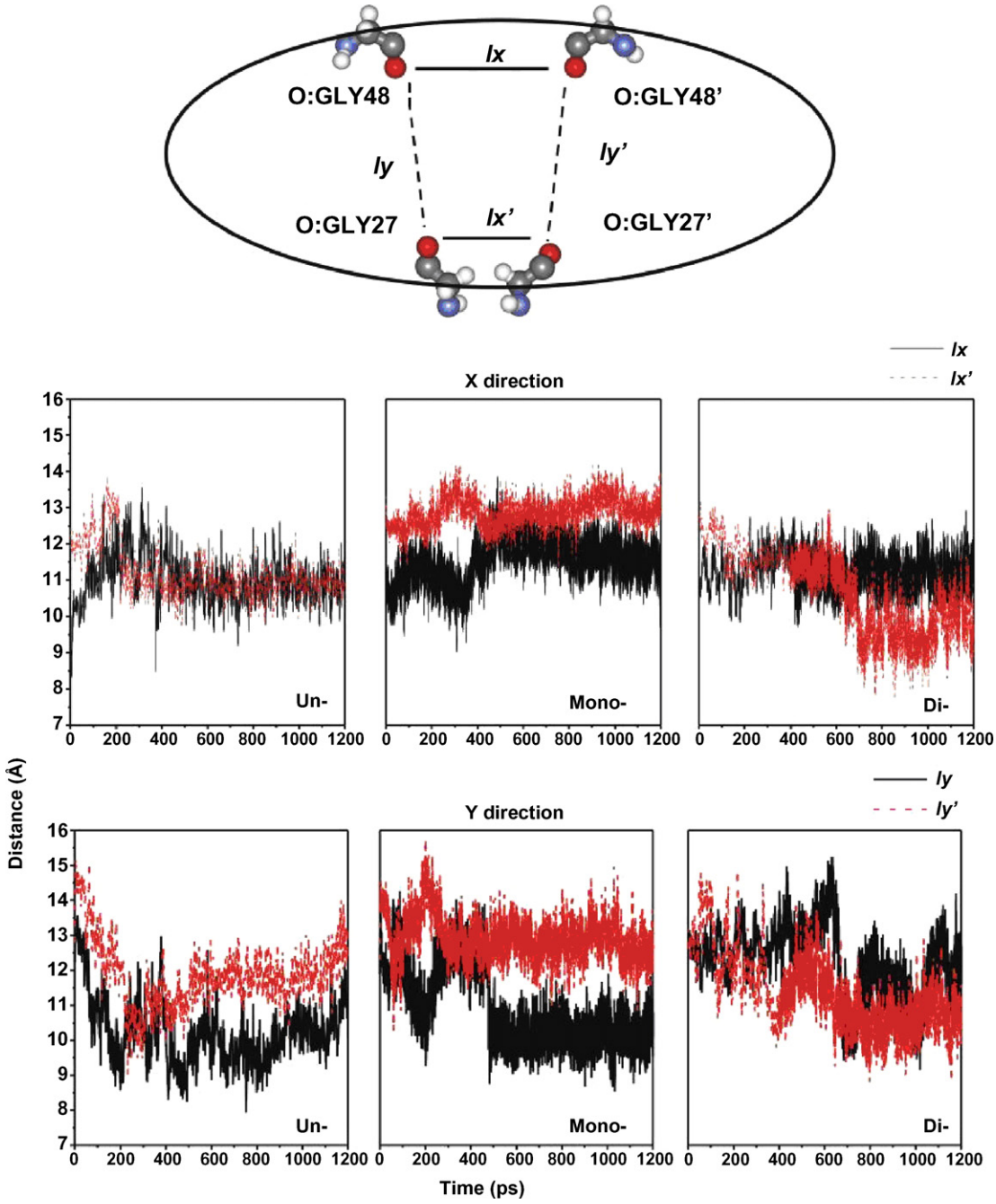

Fig. 4. Changes of the HIVP cavity of the three protonated states, defined by the four distances between oxygen atoms of the Gly48, Gly48′, Gly27 and Gly27′ (see text for more details).

supports this statement clearly. As can be seen from this figure that conformation as well as position of the C_{60} alcohol in the Un-state (Fig. 3, green) differs significantly from the other two states (Fig. 3, red and blue).

3.2. Changes of enzyme's cavity and the flap motion

The cavity was defined by the following distances: *lx*(O:GLY48–O:GLY48′), *lx*′ (O:GLY27–O:GLY27′), *ly*(O:GLY48–O:GLY27) and *ly*′ (O:GLY48′–O:GLY27′), see Fig. 4. Changes and flexibilities of the cavity in the three-protonation states were clearly displayed in terms of the four distances. In *x*-axis, no significant difference was observed for the *lx* distance of the three systems (solid line in Fig. 4) while the distance between the two GLY27 of both chains (*lx*′, dashed line in Fig. 4) was found in the following order: Di- $\leq$ Un- $<$ Mono-protonated systems. The later observation can be simply described by the Coulombic $COO^{-}\cdots COOH$, $COO^{-}\cdots COO^{-}$ and $COOH\cdots COOH$ interactions of the two catalytic dyad, Asp25 and Asp25′, of the Mono- Un- and Di-states, respectively. In addition, the difference between the *ly* and *ly*′ distances were, unexpectedly, detected, especially for the Un- and the Di-states in which the two Asp25 and Asp25′ residues are symmetrically protonated. This can be due only to

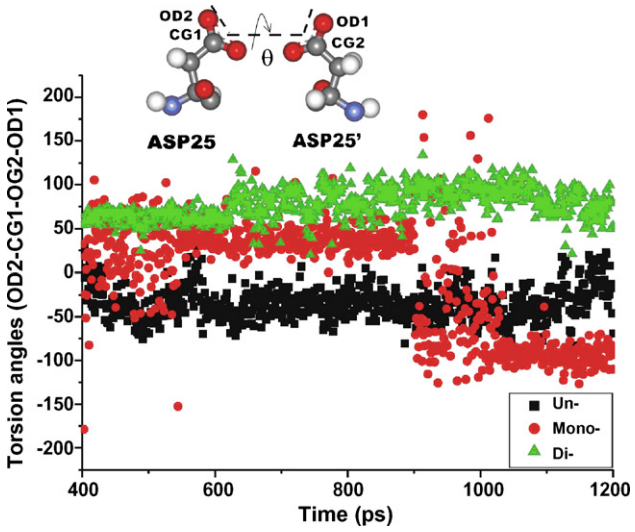

Fig. 5. Changes of the torsional angles of the catalytic dyad, Asp25 and Asp25′, defined by the OD2–CG1–CG2–OD1 for the unprotonated (Un-), monoprotonated (Mono-) and diprotonated (Di-) systems.

the orientation of the C_{60} derivative inhibitor in which its side chain was observed not to bind symmetrically to the catalytic dyad (details were described and discussed later).

Besides the cavity changes due to translational motions as shown in Fig. 4, the rotation of the –COOH and –$COOH^-$ functional groups of the catalytic dyad during 400–1200 ps was investigated and plotted in Fig. 5. The torsional angles formed by the O–C–C–O of the two carboxyl groups (see Fig. 5 for more details) show the non-planar configuration with the most frequency at about −45° for the Un-, 35° and −95° for the Mono- and 60° for the Di-systems. This indicates different conformations of the –COOH and COOH– functional groups of the two catalytic Asp25 and Asp25′ residues in the cavity of the enzyme.

To compare movement of the flap in the different protonation states, which were initially generated from the same minimized HIVP structure using close conformations, the starting and final structures of the flap were displayed in Fig. 6. The superimposition plot lies in the same viewing angle as that shown in Fig. 3. To be clearly described, the top view of the flap regions was also given in Fig. 6. As the result, the flap tips of all systems were observed to prefer the closed form. The flap configuration of the Di-state is similar to that of the initial structure where the two loops are almost parallel. This is in contrast to that of the other two states in which the flap loop of chain B was observed to lie perpendicular to that of chain A.

The above evidence was confirmed by the RMSD shown in Table 2 in which the value of 2.11 Å of the Di-state is lower than those of 2.75 and 3.06 Å of the Un- and Mono-states, respectively. This indicates the lower flap movements of the Di- than the other two states. In addition, this conclusion was also supported by the lower stabilization energy of −48.1 kcal/mol for the Di- than those of −41.7 kcal/mol for the Mono- and −45.8 kcal/mol for the Un-states. Here, the stabilization energy was calculated based on the molecular mechanics (MM) force field in AMBER—the total energy of both chains of the flap residues (residues 46–55 and 46′–55′) was subtracted by those of each chain. Taking into account all the data summarizing above, active site of the simulated complex was supposed to favor the diprotonated state.

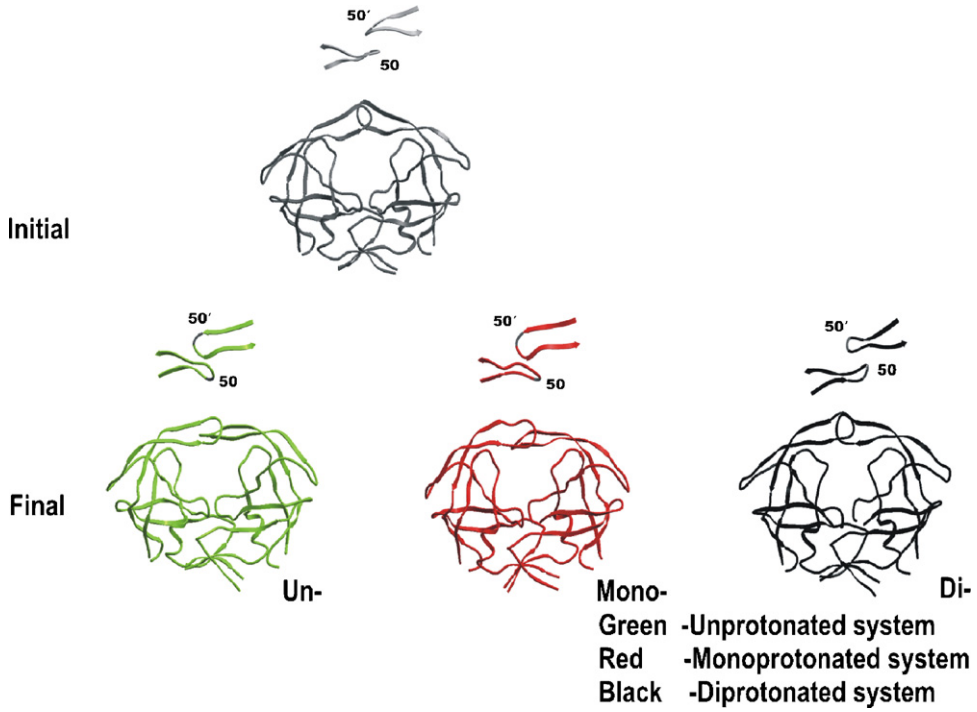

Fig. 6. The starting and final MD structures of the closed form of the HIVP in the unprotonated (Un-), monoprotonated (Mono-) and diprotonated (Di-) systems. The superimposition plot lies in the same viewing angle as that shown in Fig. 3. Top view of the flap regions was also given. The structures of the inhibitor were not shown.

3.3. Rotation of the diphenyl C_{60} alcohol

In addition to the translational motion of the diphenyl C_{60} alcohol shown in Fig. 2 in terms of its RMSD, changes of the position of the OH group were used to monitor its rotation. Here, distances from the O atom of the inhibitor to the O atom of the carboxyl group of the Asp25′ at the catalytic site (L_{OO25}) and the Ile50′ (see also Fig. 3) at the flap region (L_{OO50}) were analyzed for the three systems. The results, as a function of simulation time, were given in Fig. 7. It can be clearly seen from the plots that the OH group of the inhibitor in the Di-state (Fig. 7a, below) remains at its starting position throughout the simulation where the average L_{OO25} and L_{OO50} distances after equilibration are 5.96 and 14.93 Å, respectively (detailed investigations in terms of hydrogen bond were in the next section). Orientation of the OH bonds, extracted every 200 ps from the collected trajectories and represented by an arrow pointing from C to O atoms, CO vector, of the diphenyl C_{60} alcohol confirms the distribution of the L_{OO25} and L_{OO50} distances for the Di-state (Fig. 7b, below), very clearly.

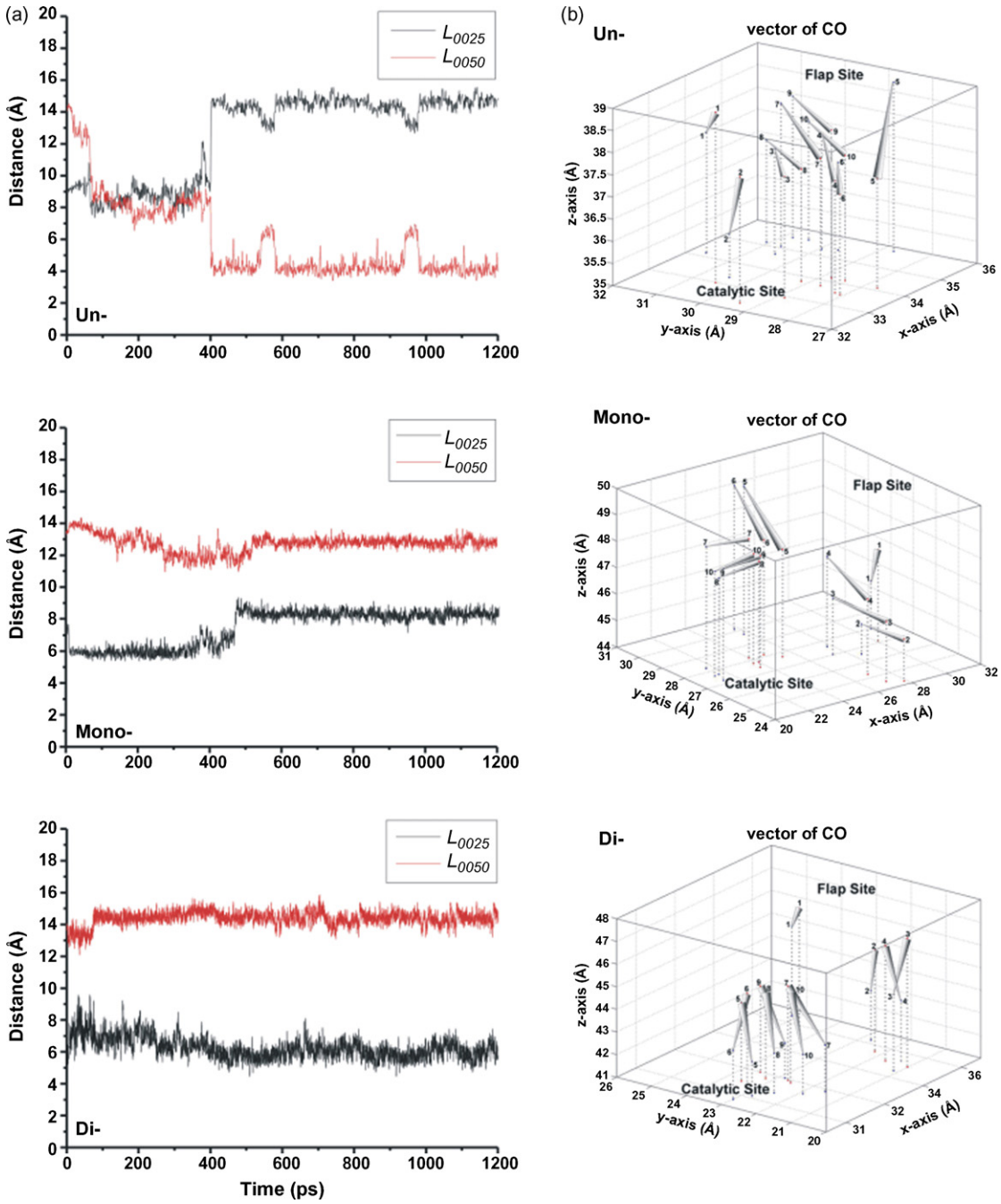

Fig. 7. (a) Changes of the distances from the O atom of the inhibitor to the O atom of the carboxyl group of the Asp25′ located at the catalytic site (L_{OO25}) and the Ile50′ located at the flap region (L_{OO50}), and (b) orientation of the vector pointing from the C to O atoms of the diphenyl C_{60} alcohol, extracted every 200 ps from the collected trajectory for the unprotonated (Un-), monoprotonated (Mono-) and diprotonated (Di-) systems.

For the Un-state, the L_{OO50} distance deceases rapidly from ~14 to ~8 Å during the first 50 ps and from ~8 to ~4 Å during 350–400 ps and remains constant afterward (Fig. 7a, top). This is in contrast to that of the L_{OO25} distance where its values increase exponentially for both ranges, 0–50 and 350–400 ps. This indicates the rotation of the C_{60} sphere, i.e., the OH group of the inhibitor in the Un-state was observed to turn from the catalytic region. Equilibration was observed to take place after 400 ps (Fig. 7a, top) with the average L_{OO25} and L_{OO50} distances of 14.43 and 5.92 Å, respectively. This is consistent with the orientation of the CO vector shown in Fig. 7b (top) where the arrow points to the catalytic dyad at the beginning, turns quickly and, then, reaches equilibrium in an area close to the flap region.

For the Mono-state (Fig. 7a, middle), the L_{OO25} distance increases slowly and remains unchanged after 400 ps. This is in contrast for the L_{OO50} distance. The average L_{OO25} and L_{OO50} distances after equilibration, 400 ps, are 8.15 and 12.67 Å, respectively. The changes indicate rotation of the OH group from its starting configuration to its preferential state where the OH group lies between the catalytic and the flap regions. The CO distribution plot (Fig. 7b, middle) agrees very well with the changes of the L_{OO25} and L_{OO50} distances. The question arises, how the diphenyl C_{60} alcohol in the Mono-state holds in place, without rotation, in the HIVP pocket. Detailed investigations were given in the next section.

3.4. Rotation of the OH group of the diphenyl C_{60} alcohol

The flexibility of the diphenyl C_{60} alcohol was displayed by the schematic representation shown in Fig. 8 in which the torsional angle defined by the OH–C68–C61–C62 (atomic labels were in an inset) was evaluated and plotted. Changes were observed significantly for the Un-state where the flip of the OH group from 65° to −150° and back starts to be detected at the first 400 ps. This synchronizes with the molecular rotation in the Un-state shown in Fig. 7a in which exponential changes of the L_{OO25} and L_{OO50} during the first 400 ps were taken place. At this configuration, where the side chain of the C_{60} lies close to the flap region, the OH group was, then, turned back to its initial position where the OH–C68–C61–C62 torsional angle is 65° and the OH group forms a hydrogen bond with the Ile50 residue in the flap region (details in the next section). In addition, changes of the torsional angle from 65° to 150° and back during the first 400 ps agree well with the separation of the RMSD for the Un-state shown in Fig. 2. However, the torsional angle of the Mono-state is fairly stable after 200 ps taken place at 30° (Fig. 8, middle) while that of the Di-state is rather flexible (Fig. 8, below).

The rotation of the OH group in the initial stage was also detected for the Mono- and Di-states (Fig. 7). This is clearly to facilitate the molecular rotation in order to move the OH group through the energy barrier due to the repulsion with the two catalytic residues. As stated in the calculation details, the OH group was initially rotated to locate between the two aspartic residues, Asp25 and Asp25′.

3.5. Hydrogen bond between HIVP and diphenyl C_{60} alcohol

Interaction between inhibitor and enzyme was monitored in terms of hydrogen bonding between their side chains. In this study, the following criteria were applied: distance between donor and acceptor non-hydrogen atoms is shorter than 4 Å and donor–acceptor-H angle is less than 60°. The results were summarized in Table 1.

The final position of the OH group of each simulated state was displayed in Fig. 9. In the Un-state, the OH group of the

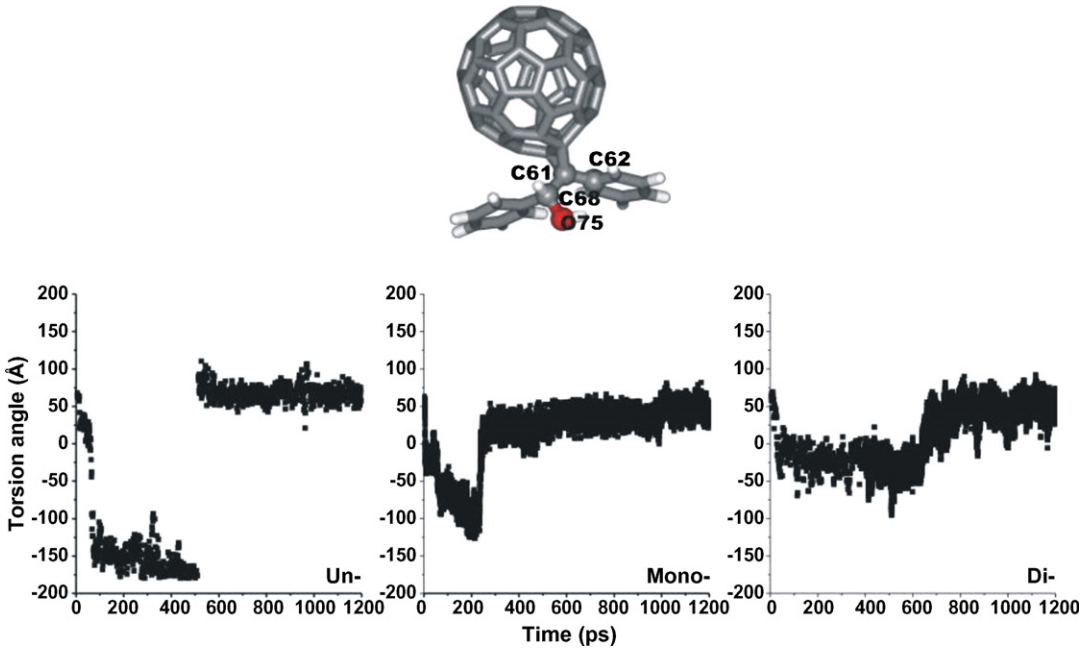

Fig. 8. Changes of the torsional angles of O75–C68–C61–C62 of diphenyl C_{60} alcohol in three protonated states.

Table 1
Possible hydrogen bonds and their characters, average distance and angle as well as percentage occupation, between HIVP and diphenyl C_{60} alcohol for the unprotonated (Un-), monoprotonated (Mono-) and diprotonated (Di-) systems

State	Hbond donor	Hbond acceptor	Average distance (Å)	Average angle (°)	%Hbond
Un-	OH:C60	O:GLY48′	3.29 (2.78–3.85)	42.63 (11.76–56.13)	3.25
	NH:Ile50′	O:C60	3.47 (2.93–4.00)	19.62 (2.73–55.39)	84.00
Mono-	OH:C60	O:Thr80	3.77 (3.06–4.00)	36.97 (10.93–57.12)	3.80
	OH:C60	O:Ile50	3.58 (2.86–3.98)	33.30 (6.21–57.01)	0.78
	NH:Ile50	O:C60	3.77 (3.27–4.00)	15.97 (0.88–47.68)	2.28
Di-	OH:C60	OD1:ASH25	2.85 (2.59–3.49)	39.54 (5.52–57.29)	3.56
	OH:C60	OD2:ASH25	3.44 (2.70–4.00)	35.16 (8.11–56.76)	1.62
	OH:C60	O:GLY27	3.47 (2.71–4.00)	37.02 (6.43–57.10)	21.56
	OH:C60	OD1:ASH25′	3.46 (2.96–3.98)	44.90 (13.78–57.18)	0.63
	O75:C60	OD2:ASH25′	3.12 (2.66–3.96)	47.98 (21.11–57.25)	3.41
	OD2–HD2:ASH25	O:C60	3.23 (2.58–4.00)	37.62 (0.28–57.26)	58.28
	NH:GLY27	O:C60	3.91 (3.83–3.96)	51.21 (47.11–55.02)	0.18
	NH:ALA28	O:C60	3.49 (2.76–4.00)	50.63 (28.52–57.28)	13.88
	OD2–HD2:ASH25′	O:C60	2.95 (2.50–3.99)	24.72 (0.62–57.06)	97.14

inhibitor was observed to form a hydrogen bond with the Ile50′ in the flap region with 84% occupation. The H atom of the OH from hydrogen bonding to the backbone nitrogen atom of Ile50′ with the corresponding distance is 3.47 Å. This conformation is similar to that of the docking structure reported by Friedman et al. [1]. Other very weak hydrogen bonds (3% occupation and bond distance is 3.29 Å) were found between Gly48′ and diphenyl C_{60} alcohol. For the Mono-state, very weakly bound between the side chains of the C_{60} and the Ile50 and Thr80 residues were detected with the hydrogen bond occupation percentage below 4%. It is interesting to note here, therefore, that the diphenyl C_{60} alcohol was observed to form indirect hydrogen bonds with the Ile50′ via water molecules (details were in the next section). For the Di-state, the functional group of the inhibitor was bound to the enzyme active site throughout the simulation with 97% and 58% occupations and the average hydrogen bond distances to the Asp25′ and the Asp25 of 2.95 and 3.23 Å, respectively (see Table 1 and Fig. 9, right). The above structural data implies that binding to both flap and catalytic regions might improve the inhibition constant of the C_{60}-based inhibitor. This is supported by the experimental data, which suggested that the EC_{50} of the C_{60}-based inhibitor with two side chains in the *trans*-isomer is significantly lower than that of the *cis*-isomer [4]. The corresponding EC_{50} for both forms are 0.21 and 2.5 μM, respectively. The molecular geometry of the *trans*-form allows one side chain to bind to the catalytic site while the other binds to the flap residue.

The hydrogen bond data shown in Table 1 and snapshot of the preferential conformation of the diphenyl C_{60} alcohol (Fig. 9) support the conclusion on the rotation of the C_{60} molecule (Fig. 7) and the OH group (Fig. 8) in the three protonated states very well. In other words, changes of the L_{OO25} and L_{OO50} distances (Fig. 7) due to the molecular rotation from its initial (where the side chain of the inhibitor locates between the catalytic dyad) to the equilibrium configurations correspond to the snapshot shown in Fig. 9, i.e., rotation takes

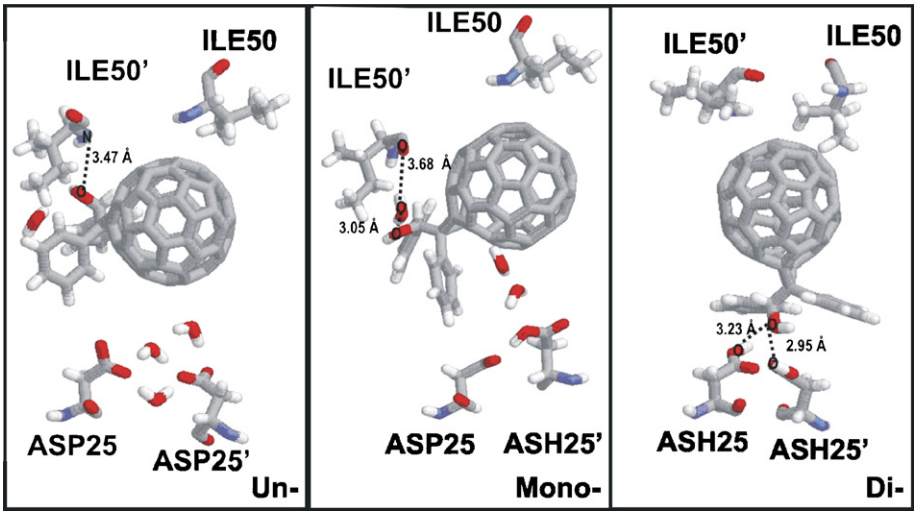

Fig. 9. Schematic representation of the hydrogen bond distances between the OH groups of the fullerene-based inhibitor and the amino acid residues of enzyme in the Un- Mono- (bonding through water molecule) and Di-systems.

place for the Un-more than the Mono- and the Di-states, respectively. In addition, this order is the same as the changes due to the OH rotation (Un- > Mono- > Di-) shown in Fig. 8.

According to the structural data of the three protonation states, sidechain orientations of the Ile50/Ile50′ in the Di-state are significantly different from those in the Un- and Mono-state. This implies a substantial difference in conformation of the HIV-1 protease flap. Importantly, RMSD values separate in Table 2 indicated that flap structure of the Di-state has the flap structure most similar to the crystal structure. Additionally, it is generally recognized that the binding pattern of the HIV-1 protease–inhibitor complexes is characterized by the interactions between the active site residues Asp25/Asp25′ and the hydroxyethylene isostere protease inhibitor [43,44]. These results suggested us to conclude that the active site of the HIVP complexed with the diphenyl C_{60} alcohol is the diprotonation states.

An above conclusion on the protonation state of the complex is supported by a direct correlation between the activity of inhibitor and the amount of hydrophobic surface area proposed by Friedman et al. [1–3]. Therefore, the specific conformational rearrangements within the cavity region around the spherical C_{60} would facilitate and strengthen its hydrophobic interactions with the active site residues. The inhibitor's molecular rearrangements, which are exhibited by the rotations of the C_{60} molecule in Fig. 7 and of the OH bond in Fig. 8 led to the final configuration in Fig. 9, are due to the difference in the hydrophobic interaction between the catalytic regions of the three protonated states and the side chain of the diphenyl C_{60} alcohol.

In addition, HIVP consists of four hydrophobic pockets near its active sites and favorable hydrophobic interactions with these pockets are desirable for an inhibitor to achieve nanomolar potency [45]. It was also found that the two benzene rings at the side chain of the diphenyl C_{60} alcohol contribute hydrophobicity over the OH functional group. This statement was clarified by the atomic-based hydrophobicity calculation based on a scoring function method developed by Wang's group [32]. The hydrophobic values of each atom were parameterized from the log *P* value of hundreds of organic compounds. The positive hydrophobicity value of 2.62 for the side chain of diphenyl C_{60} alcohol supports an above assumption.

3.6. Solvent molecule in the catalytic pocket of the HIVP

The catalytic mechanism of the protease is most likely a combination of favorable binding of inhibitor with enzyme and the role of water molecules in the enzyme pocket. Often, a water molecule is needed in order to facilitate proton transfer in the catalytic process. To monitor water position and orientation in the cavity of the HIVP pocket as well as to examine reliability of the force field parameters in representing an explicit water model used, atom–atom radial distribution functions (RDFs, $g_{i-j}(r)$) centered (the *i*th atom) at the four catalytic carboxylate oxygens (OD1 and OD2) of the catalytic dyad (Asp25 and Asp25′) and the oxygen of diphenyl C_{60} alcohol (O75) were evaluated. Here, *j* denotes the oxygen atoms of water molecules. The plots give information on the probability of finding the oxygen atoms of water molecules around the *i*th atom. Calculations were performed separately for the three different protonated states. The results were given in Fig. 10. Integration number, $n(r)$, up to the first minimum of each RDF was also calculated and given. Note that tail of the RDF shown in this figure does not approach unity because the simulated systems are not homogeneous, i.e., large part of the simulation box was occupied by the inhibitor–enzyme complex. This is in contrast to those of the small molecular systems.

Almost all RDFs from the carboxylate oxygens show sharp first peaks centered at about 2.8 Å. This indicates the hydrogen bonding between water and the two catalytic residues. As expected, the RDFs for the Asp25 (Fig. 10, dashed line) and Asp25′ (Fig. 10, solid line) of the Un- and Di-states are very similar whereas those of the unsymmetrical monoprotonated state show different characters. Integrate up to the first minimum of each RDF leads to the first shell coordination numbers of 3, 1.5 and 0 water molecules for the Un-, Mono-, and Di-protonated systems, respectively. Tightly bound water molecules were indicated by the height, sharpness and the distance to the first maximum of the RDFs. With these criteria, the simulation results indicate the following order of the stability of water-enzyme binding: Di- < Mono- < Un-states. Comments should be made concerning the overlapping of the RDFs centered at the Asp25 and Asp25′. Therefore, the same water molecules were detected to locate under the first peak of the two RDFs, centered at the carboxylate oxygens of the Asp25 and Asp25′.

For the RDFs centered at the O atoms of the OH group of the inhibitor (O75), those of the Un- and Mono-states show pronounced first maximum at ∼2.8 Å (Fig. 10a and b, right). The corresponding coordination number integrated up to the first minimum of each RDF is 1 water molecule. These facts lead to a clear conclusion that a water molecule forms hydrogen bonds with the OH group of the inhibitor with the O···O distance of ∼2.8 Å. Snapshots were in Fig. 9 where the detected waters for the Un- and the Mono-states were displayed. The inhibitor–water and water–Ile50′ O···O distances in Mono-state are 3.05 and 3.68 Å, respectively. Interestingly, this water molecule in the Mono-state was observed also to form hydrogen bonds simultaneously with the Ile50′ residue of the HIVP. This is a clear answer to the question mentioned in the previous section that how the diphenyl C_{60} alcohol in the Mono-state holds in place, without rotation, in the HIVP pocket. Note that the radius of 5–6 Å from the OD1, OD2 and

Table 2
The RMSD values of HIVP flap's residues (chain A/chain B) compared between X-ray structure (1AID) and MD snapshot of each state

Residues	RMSD (Å)		
	Un-state	Mono-state	Di-state
48/48′	0.86/1.22	1.50/1.62	2.63/2.09
49/49′	3.17/1.35	3.37/2.14	2.84/1.60
50/50′	3.07/2.84	2.74/4.21	1.86/1.41
51/51′	2.09/5.73	1.73/5.77	1.32/1.31
52/52′	1.20/4.03	1.54/3.88	1.54/1.31

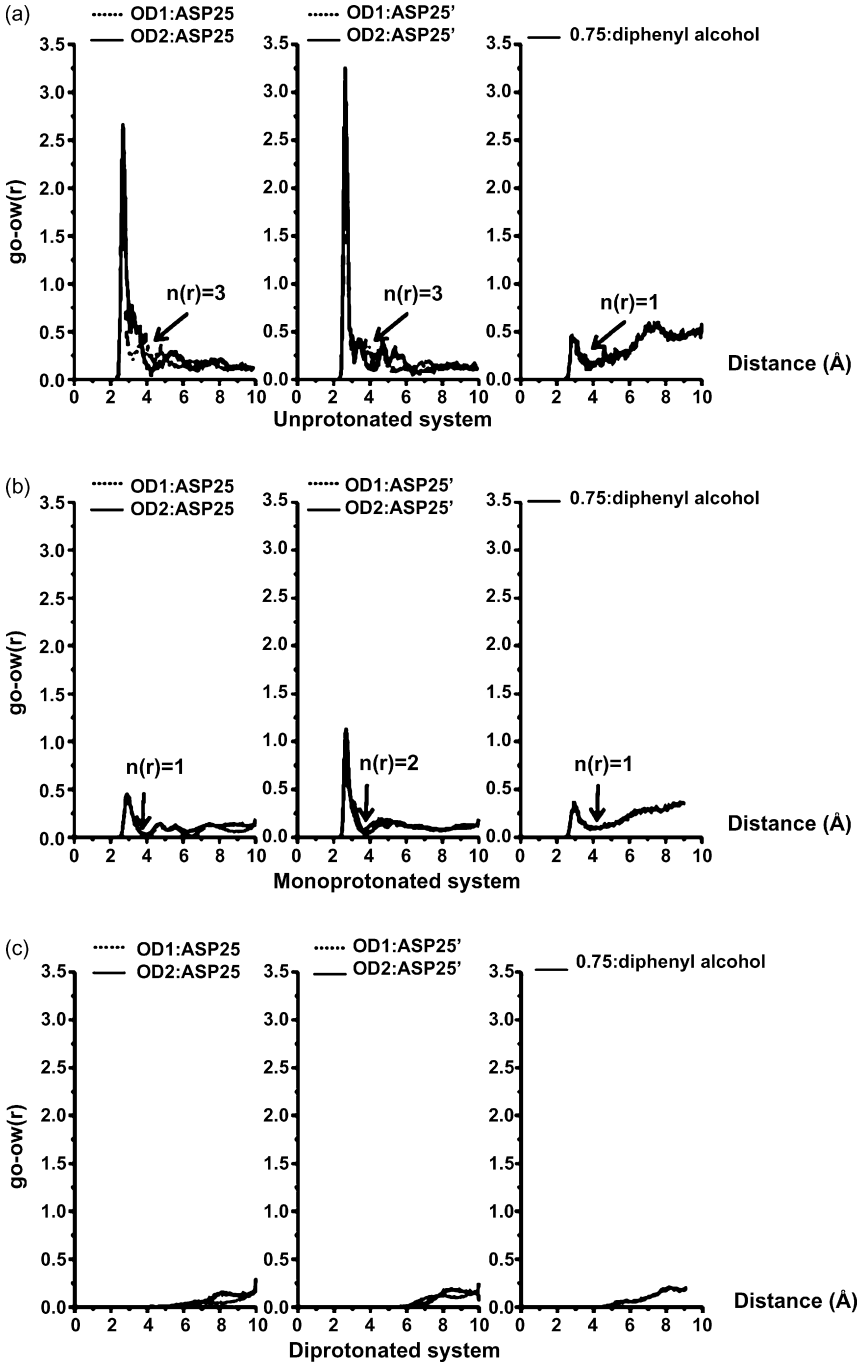

Fig. 10. Atom–atom radial distribution function, $g_{i-j}(r)$, centered at the ith atom, which are the four catalytic carboxylate oxygens (OD1 and OD2) of the catalytic dyad (Asp25 and Asp25′) and the oxygen of diphenyl C_{60} alcohol (O75) while j denotes oxygen atom of water molecule. The corresponding integration number, $n(r)$, up to the first minimum (marked by arrow) of each RDF was also given.

O75 of the Di-state (see Fig. 10c), no water molecule was detected. A clear description for this observation is the snapshot shown in Fig. 9 (right). Here, optimal orientation of the diphenyl C_{60} alcohol takes place in the configuration where its OH group was located between the catalytic dyad, i.e., the OH group forms hydrogen bonds with the aspartic residues with the O···O distances to the Asp25 and Asp25′ of 3.23 and 2.95 Å, respectively.

Some comments should be made concerning the complete desolvation of the active site complexed with inhibitor in the diprotonated state seems in contrast to that found from the molecular dynamic study by Zhu et al. [26]. However, it was also reported that water molecule in the catalytic site of the Di- was significantly lower than those of Un- and Mono-states. This discrepancy can be understood by the different final-orientation of the inhibitor obtained from our and Zhu's simulations. In our study, the initial configuration of the OH group of the three simulated systems was manually turned to locate between the two aspartics. The stabilization energy of the Di-state for this configuration is ∼60 kcal/mol lower than that obtained from the

docking procedure (see Section 3.1). This is different from that published by Zhu et al. where the starting configuration was generated from the molecular docking and the OH group can not move through such high energy barrier to form a hydrogen bond with the aspartic's carbonyl. The average distance between the OH oxygen on inhibitor and the four catalytic oxygens in the active site Asp dyad reported by Zhu is 5.12 Å. Consequently, water can easily approach and form a hydrogen bond with the catalytic site.

The solvation data shown above supports the conclusion that the Di-system is the preferential protonation state. As it is known that no water molecule is available in the catalytic site of the HIVP complexed with FDA-approved hydroxyethylene isostere inhibitors [44,45]. This is consistent with the RDF plots shown in Fig. 10 in which no water molecule was detected in the catalytic cavity of the Di-protonation state.

4. Conclusions

The MD simulations for three protonation systems of aspartic acid active site provides the significant conformational change in structure of enzyme and inhibitor in order to allow the optimum fit in binding with fullerene-based inhibitor. To our best knowledge, this is the first microscopic investigation that observed the binding orientation in the dynamic equilibrium structure due to the possible hydrogen bonding of C_{60}-based inhibitor to the flap region beside the hydrophobic characteristic of C_{60} that fit well to the HIVP's cavity and the hydrogen bonding at the catalytic aspartate. Besides the complex conformational energy and hydrophobic interaction between the C_{60} moiety and the interior of the cavity, the protonation state of active sites has an effect on the complex conformation. As the protonation state of HIVP-C_{60} derivatives does not provide by any experimental data, our results lead to a conclusion that the Di-state is the preferential protonation state. This information is known to be a prerequisite for the structure-based drug design.

The structural analysis showed the possible hydrogen bonding between diphenyl C_{60} alcohol and amino acid residue in flap specific to one chain of Un- and Mono-protonated HIVP system in the equilibrium whereas the stable hydrogen bonding to the active site was found in the di-protonated HIVP system. The structural data on the binding and orientation of the C_{60}-based inhibitor in the cavity of HIVP would be helpful to design more potent inhibitor. In addition, we calculated the possible number of water molecules in the active site regions in terms of RDF between catalytic oxygen of aspartic acid and oxygen water molecules in the presence of fullerene-based inhibitor. The result showed the relationship between the number of water molecules and the protonation state of the active site. No water molecule in the active site was found in the diprotonated system. Interestingly, the inhibitors in the Un-systems were indirectly bridged to the flap and in Mono-system were bridged through water molecule, confirmed RDF plot between the oxygen of diphynyl C_{60} alcohol and the O of water. Our simulations nevertheless provide valuable information for the design of improved HIVP inhibitors based upon this lead compound.

Acknowledgments

We gratefully acknowledge a generous grant of computer time from the Computation Chemistry Unit Cell (CCUC), Faculty of Science, Chulalongkorn University, Bangkok, Thailand, where the simulations were performed on a cluster of 8 Intel P4 processors. We also acknowledge Dr. Vudhichai Parasuk, Dr. Somsak Pianwanit, Department of Chemistry, Faculty of Science, Chulalongkorn University and Dr. Tawun Remsungnen, Department of Mathematics, Faculty of Science, Khon Kaen University, for many useful discussions. This project was supported by the Post Doctorate Research Fund and the TRF Senior Research Scholarship, the Thailand Research Fund (TRF), and partly funded by Center for Innovation in Chemistry: Postgraduate and Research Program in Chemistry (PERCH-CIC), Thailand.

References

[1] S.H. Friedman, D.L. De Camp, R.P. Sijbesma, G. Srdanov, F. Wudl, G.L. Kenyon, Inhibition of the HIV-1 protease by fullerene derivatives: model building studies and experimental verification, J. Am. Chem. Soc. 115 (1993) 6506–6509.
[2] R. Sijbesma, G. Srdanov, F. Wudl, J.A. Castoro, C. Wilkins, S.H. Friedman, D.L. DeCamp, G.L. Kenyon, Synthesis of a fullerene derivative for the inhibition of HIV enzymes, J. Am. Chem. Soc. 115 (1993) 6510–6512.
[3] S.H. Friedman, P.S. Ganapathi, Y. Rubin, G.L. Kenyon, Optimizing the binding of fullerene inhibitors of the HIV-1 protease through predicted increases in hydrophobic desolvation, J. Med. Chem. 41 (1998) 2424–2429.
[4] S. Marchesan, T. Da Ros, G. Spalluto, J. Balzarini, M. Prato, Anti-HIV properties of cationic fullerene derivatives, Bioorg. Med. Chem. Lett. 15 (2005) 3615–3618.
[5] R.M. Klabe, L.T. Bacheler, P.J. Ala, S. Erickson-Viitanen, J.L. Meek, Resistance to HIV protease inhibitors: a comparison of enzyme inhibition and antiviral potency, Biochemistry 37 (1998) 8735–8742.
[6] M. Brettreich, A. Hirsch, A highly water-soluble endro [60] fullerene, Tetrahedron Lett. 39 (1998) 2731–2734.
[7] R.F. Schinazi, R. Sijbesma, G. Srdanov, C.I. Hill, F. Wudl, Synthesis and virucidal activity of a water-soluble, configurationally stable, Antimicrob. Agents Chemother. 37 (1993) 1707–1710.
[8] D.I. Schuster, S.R. Wilson, R.F. Schinazi, Anti-human immunodeficiency virus Activity and cytotoxicity of derivatizedbuckinsterfullerenes, Bioorg. Med. Chem. Lett. 6 (1996) 1253–1256.
[9] S.H. Friedman, R.F. Schinazi, F. Wudl, C.I. Hill, D.L. DeCamp, R. Sijbesma, G.L. Kenyon, U.S. Patent 5 (1998) 811, 460.
[10] D.L. Surleraux, H.A. de Kock, W.G. Verschueren, G.M. Pille, L.J. Maes, A. Peeters, S. Vendeville, S. De Meyer, H. Azijn, R. Pauwels, M.P. de Bethune, N.M. King, M. Prabu-Jeyabalan, C.A. Schiffer, P.B. Wigerinck, Design of HIV-1 protease inhibitors active on multidrug-resistant virus, J. Med. Chem. 48 (2005) 1965–1973.
[11] M. Miller, J. Schneider, B.K. Sathyanarayana, M.V. Toth, G.R. Marshall, L. Clawson, L. Selk, S.B.H. Kent, A. Wlodawer, Direct and remote sensing observations of the effects of ships on clouds, Science 246 (1989) 1146–1149.
[12] Y.C. Lin, Z. Beck, T. Lee, V.D. Le, G.M. Morris, A.J. Olson, C.H. Wong, J.H. Elder, Alteration of substrate and inhibitor specificity of feline immunodeficiency virus protease, J. Virol. 74 (2000) 4710–4720.
[13] L.K. Nicholson, T. Yamazaki, D.A. Torchia, S. Grzesiek, A. Bax, S.J. Stahl, J.D. Kaufman, P.T. Wingfield, P.Y.S. Lam, P.K. Jadhav, C.N. Hodge, P.J. Domaille, C.H. Chang, Flexibility and function in HIV-1 protease, Nat. Struct. Biol. 2 (1995) 274–280.

[14] S.W. Rick, J.W. Erickson, S.K. Burt, Reaction path and free energy calculations of the transition between alternate conformations of HIV-1 protease, Proteins Struct. Funct. Genet. 32 (1998) 7–16.
[15] R. Ishima, D.I. Freedberg, Y.X. Wang, I. Kustanovich, J.M. Louis, D.A. Torchia, Flap opening and dimer-interface flexibility in the free and inhibitor-bound HIV protease, and their implications for function, Structure 7 (1999) 1047–1055.
[16] W.R.P. Scott, C.A. Schiffer, Curling of flap tips in HIV-1 protease as a mechanism for substrate entry and tolerance of drug resistance, Structure 8 (2000) 1259–1265.
[17] D.I. Freedberg, R. Ishima, J. Jacob, Y.X. Wang, I. Kustanovich, J.M. Louis, D.A. Torchia, Rapid structural fluctuations of the free HIV protease flaps in solution: relationship to crystal structures and comparison with predictions of dynamics calculations, Protein Sci. 11 (2002) 221–232.
[18] B.Y. Ma, M. Shatshy, H.J. Wolfson, R. Nussinov, Multiple diverse ligands binding at a single protein site: a matter of pre-existing populations, Protein Sci. 11 (2002) 184–197.
[19] H.A. Carlson, J.A. McCammon, Accommodating protein flexibility in computational drug design, Mol. Pharmacol. 57 (2000) 213–218.
[20] S.H. Friedman, G.L. Kenyon, R.F. Schinazi, R.P. Sijbesma, D.L. DeCamp, F. Wudl, C. Hill, Water soluble fullerenes with antiviral activity, U.S. Patent 5 (1998) 811, 460.
[21] G.L. Marcorin, T. Da Ros, S. Castellano, G. Stefancich, I. Bonin, S. Miertus, M. Prato, Design and synthesis of novel [60] fullerene derivatives as potential HIV aspartic protease inhibitors, Org. Lett. 2 (2000) 3955–3958.
[22] S. Bosi, T. Da Ros, G. Spalluto, I. Balzarini, M. Prato, Synthesis and anti-HIV properties of new water-soluble bis-functionalized [60] fullerene derivatives, Bioorg. Med. Chem. Lett. 13 (2003) 4437–4440.
[23] A. Bianco, C. Corvaja, M. Crisma, D.M. Guldi, M. Maggini, E. Sartori, C. Toniolo, A helical peptide receptor for [60] fullerene, Chemistry 8 (2002) 1544–1553.
[24] A. Bianco, T. Da Ros, M. Prato, C. Toniolo, Fullerene-based amino acids and peptides, J. Pept. Sci. 7 (2001) 208–219.
[25] T. Mashino, K. Shimotohno, N. Ikegami, D. Nishikawa, K. Okuda, K. Takahashi, S. Nakamura, M. Mochizuki, Human immunodeficiency virus-reverse transcriptase inhibition and hepatitis C virus RNA-dependent RNA polymerase inhibition activities of fullerene derivatives, Bioorg. Med. Chem. Lett. 15 (2005) 1107–1109.
[26] Z. Zhu, D.I. Schuster, M.E. Tuckerman, Molecular dynamics study of the connection between flap closing and binding of fullerene-based inhibitors of the HIV-1 protease, Biochemistry 42 (2003) 1326–1333.
[27] R. Smith, I.M. Brereton, R.Y. Chai, S.B. Kent, Ionization states of the catalytic residues in HIV-1 protease, Nat. Struct. Biol. 3 (1996) 946–950.
[28] S. Piana, D. Sebastiani, P. Carloni, M. Parrinello, Ab initio molecular dynamics-based assignment of the protonation state of pepstatin A/HIV-1 protease cleavage site, J. Am. Chem. Soc. 123 (2001) 8730–8737.
[29] V. Hornak, A. Okur, R.C. Rizzo, C. Simmerling, HIV-1 protease flaps spontaneously open and reclose in molecular dynamics simulations, Proc. Natl. Acad. Sci. U.S.A. 103 (2006) 915–920.
[30] V. Hornak, A. Okur, R.C. Rizzo, C. Simmerling, HIV-1 protease flaps spontaneously close to the correct structure in simulations following manual placement of an inhibitor into the open state, J. Am. Chem. Soc. 128 (2006) 2812–2813.
[31] M. Layten, V. Hornak, C. Simmerling, The open structure of a multi-drug-resistant HIV-1 protease is stabilized by crystal packing contacts, J. Am. Chem. Soc. 128 (2006) 13360–13361.
[32] R. Wang, L. Lai, S. Wang, Further development and validation of empirical scoring functions for structure-based binding affinity prediction, J. Comput. Aided Mol. Des. 16 (2002) 11–26.
[33] D.A. Case, J.C.D. Pearlman, T. Cheatham III, J. Wang, W. Ross, C. Simmerling, T.D.T. Merz, R. Stanton, A. Cheng, J. Vincent, M. Crowley, V.T.H. Gohlke, R. Radmer, Y. Duan, J. Pitera, I. Massova, G. Seibel, U.C.S.P. Weiner, P.A. Kollman, AMBER 7, University of California, San Francisco, CA, 2002.
[34] D.A. Pearlman, D.A. Case, J.W. Caldwell, W.S. Ross, T.E. Cheatham III, S. DeBolt, D. Ferguson, G. Seibel, P.A. Kollman, AMBER, a package of computer programs for applying molecular mechanics, normal mode analysis, molecular dynamics and free energy calculations to simulate the structural and energetic properties of molecules, Comp. Phys. Commun. 91 (1995) 1–41.
[35] S. Promsri, P. Chuichay, V. Sanghiran, V. Parasuk, S. Hannongbua, Molecular and electronic properties of HIV-1 protease inhibitor C60 derivatives as studied by the ONIOM method, J. Mol. Struct.: THEOCHEM 715 (2005) 47–53.
[36] D.S. Goodsell, A.J. Olson, Automated docking of substrates to proteins by simulated annealing, Proteins Struct. Funct. Genet. 8 (1990) 195–202.
[37] G.M. Morris, D.S. Goodsell, R. Huey, A.J. Olson, Distributed automated docking of flexible ligands to proteins: parallel applications of AutoDock 2.4, J. Comput. Aided Mol. Design 10 (1996) 293–304.
[38] G.M. Morris, D.S. Goodsell, R.S. Halliday, R. Huey, W.E. Hart, R.K. Belew, A.J. Olson, Automated docking using a lamarckian genetic algorithm and an empirical binding free energy function, J. Comp. Chem. 19 (1998) 1639–1662.
[39] R. Lappatto, T. Blundell, A. Hemmings, J. Overington, A. Wilderspin, S. Wood, J.R. Merson, P.J. Whittle, D.E. Danley, K.F. Geoghegan, S.J. Hawrylik, S.E. Lee, K.G. Scheld, P.M. Hobart, X-ray analysis of HIV-1 proteinase at 2.7 Å resolution confirms structural homology among retroviral enzymes, Nature (London) 342 (1989) 299–302.
[40] M.A. Navia, P.M.D. Fitzgerald, B.M. McKeever, C.T. Leu, J.C. Heimbach, W.K. Herber, I.S. Sigal, P.L. Darke, J.P. Springer, Three-dimensional structure of aspartyl protease from human immunodeficiency virus HIV-1, Nature (London) 337 (1989) 615–620.
[41] M.L. West, D.P. Fairlie, Targeting HIV-1 protease: a test of drug-design methodologies, Trends Pharmacol. Sci. 16 (1995) 67–75.
[42] H.J.C. Berendsen, J.P.M. Postma, W.F. van Gunsteren, A. DiNola, J.R. Haak, Molecular dynamics with coupling to an external bath, J. Comp. Phys. 81 (1984) 3684–3690.
[43] A. Wlodawer, J. Vondrasek, Inhibitors of HIV-1 protease: a major success of structure-assisted drug design, Annu. Rev. Biophys. Biomol. Struct. 27 (1998) 249–284.
[44] A. Brik, C. Wong, HIV-1 protease: mechanism and drug discovery, Org. Biomol. Chem. 1 (2003) 5–14.
[45] C. Debouck, The HIV-1 protease as a therapeutic target for AIDS, AIDS Res. Hum. Retrovirus. 8 (1992) 153–164.